

Review

# Photoelectrochemical Device Designs toward Practical Solar Water Splitting: A Review on the Recent Progress of $\text{BiVO}_4$ and $\text{BiFeO}_3$ Photoanodes

Sang Yun Jeong, Jaesun Song and Sanghan Lee \* 

School of Materials Science and Engineering, Gwangju Institute of Science and Technology,  
123 Cheomdangwagi-ro, Buk-gu, Gwangju 61005, Korea; sangyunj78@gist.ac.kr (S.Y.J.); jaesun12@gist.ac.kr (J.S.)

\* Correspondence: sanghan@gist.ac.kr; Tel.: +82-62-715-2314

Received: 26 July 2018; Accepted: 13 August 2018; Published: 17 August 2018



## Featured Application: Nanomaterials for Solar Water Splitting

**Abstract:** Solar-driven water splitting technology is considered to be a promising solution for the global energy challenge as it is capable of generating clean chemical fuel from solar energy. Various strategies and catalytic materials have been explored in order to improve the efficiency of the water splitting reaction. Although significant progress has been made, there are many intriguing fundamental phenomena that need to be understood. Herein, we review recent experimental efforts to demonstrate enhancement strategies for efficient solar water splitting, especially for the light absorption, charge carrier separation, and water oxidation kinetics. We also focus on the state of the art of photoelectrochemical (PEC) device designs such as application of facet engineering and the development of a ferroelectric-coupled PEC device. Based on these experimental achievements, future challenges, and directions in solar water splitting technology will be discussed.

**Keywords:** oxide semiconductor; bismuth vanadate; bismuth ferrite; hematite; plasmonic effect; heterostructure film; gradient doping; oxygen evolution catalyst; facet engineering; ferroelectric

## 1. Introduction

Energy harvesting technology with a clean and renewable source of energy has drawn significant attention because of its possibility for solving the global energy challenge. Among the renewable energy sources including solar, wind, geothermal, and hydropower energy, solar seems the most desirable since it can support future societies in a sustainable way with the use of hydrogen gas as an energy carrier [1]. Along with that consideration, the solar-derived hydrogen production from water such as photoelectrochemical (PEC) water splitting has made significant progress [2,3]. In general, the PEC water splitting system consists of photoelectrodes (photoanode or photocathode), electrolyte, and a light source. Mostly, light-absorbing semiconductors have been used as the photoelectrode, and the electrode materials have been being of great interest in the field of PEC water splitting. Among various materials, this review focuses on bismuth vanadate ( $\text{BiVO}_4$ ) and bismuth ferrite ( $\text{BiFeO}_3$ ) which are small band gap oxide semiconductors. There are some advantages of using  $\text{BiVO}_4$  and  $\text{BiFeO}_3$  as the photoanode. Briefly, they are composed of inexpensive elements and they can utilize visible light. The latter becomes more important when they utilize the solar radiation on earth, since about half of the radiation on earth corresponds to the visible light. However, they suffer from excessive charge carrier recombination, poor charge transport, and slow water oxidation kinetics. In order to solve the problems, various efforts have been investigated and the detailed strategies will be discussed further in Section 2. The electrolyte in the PEC water splitting mainly consists of water, and the use of seawater as the unlimited feedstock

for the production of hydrogen might be allowed through the investigation, using an aqueous solution of salts as the electrolyte. With a simulated one sun radiation from the light source, the PEC water splitting processes take place with several steps as follows (also see Figure 1):

1. Absorption of solar radiation by the photoelectrode, followed by charge carrier generation as a result of photoexcitation of electrons in the valence band of photoelectrode;
2. Separation and transport of charge carriers to the electrode surface by the internal or external bias applied through the circuit;
3. Oxidation of water at the anode by the photoexcited holes. Simultaneously, transport of  $H^+$  ions from the anode to the cathode, and transport of the photoexcited electrons to the cathode through an external circuit, followed by the reduction of  $H^+$  ions into hydrogen gas at the cathode by the photoexcited electrons.

As a result of the series of steps in the PEC water splitting, the solar energy can be converted into the hydrogen gas as the chemical fuel. The bottleneck for the realization of efficient and practical water splitting systems lies on the way to (1) effective charge carrier generation and separation, and (2) rapid water redox kinetics. The overall process is represented in Figure 1 with the PEC water splitting system consists of the photoanode and the metal counterpart as the cathode. More detailed issues on each step process and the strategies for efficient PEC devices will be discussed in Sections 2 and 3.

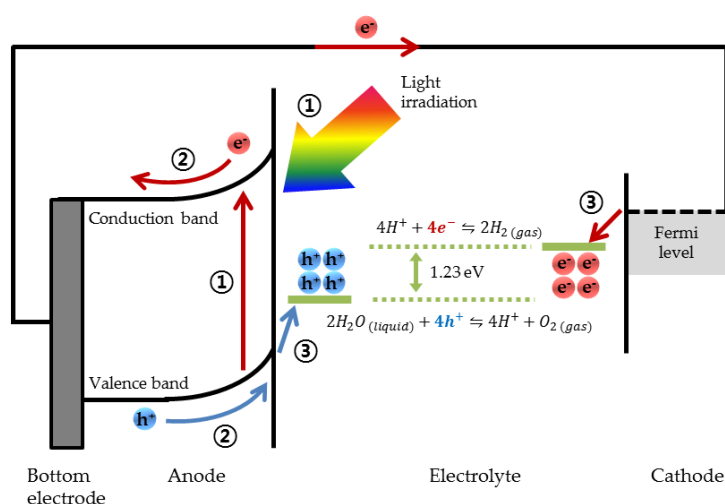


**Figure 1.** Schematic representation of the photoelectrochemical (PEC) water splitting process in a common PEC water splitting system consisting of a photoanode and a metal counterpart.

This review seeks to provide the reader with the PEC device designs to improve the water splitting activity, and thereby aids the design of a highly efficient PEC device for practical solar water splitting. On one hand, the inherent problems including electron-hole recombination in bulk and on a small surface area per unit volume, which limits the activity of thin film photocatalysts in comparison with the porous and nanostructured morphologies (e.g., nanowires). On the other hand, as a model structure, the thin film configuration gives advantages that the understanding of complex relations between the light absorption, the charge separation, and the water redox kinetics becomes simple. In this regard, the review focuses on these investigations using thin film photocatalysts. In the next section, the review starts with describing the step processes including light absorption, the carrier separation and transport, and the water oxidation kinetics, respectively. After then, the discussions will be focused on the PEC device designs for investigating the enhancement of the water splitting reaction, that lead us to achieve more efficient water splitting devices. Another aim of the review is to introduce the state-of-the-art of PEC device designs; for example, the application of facet engineering and the development of ferroelectric-coupled PEC devices.

## 2. Strategies and Device Designs for Efficient PEC Water Splitting

### 2.1. Absorption of Solar Radiation

After the first report on photocatalytic water splitting by Fujishima and Honda [4],  $\text{TiO}_2$  had been focused upon as pioneer photocatalyst at the early-stage of development because of its abundance and its good resistance to various chemicals. In the same manner, considering that PEC water splitting is generally conducted using the aqueous solutions containing organic salts, various oxide semiconductors have been used as photoelectrodes, owing to its excellent chemical resistance. However, the large band gap energy of most oxide semiconductors limits the absorption of light to the near-UV region. Thus, the poor photocatalytic performances have been considered as a significant problem. In order to solve the problem, many researchers have endeavored to discover small band gap oxide semiconductors. As a result of such efforts, a few candidates have been introduced and investigated extensively. The promising candidates are  $\text{BiVO}_4$  [5–24],  $\text{Fe}_2\text{O}_3$  [25–32], and  $\text{BiFeO}_3$  [33–35]. Figure 2 shows the band gap energies and band edge positions of various semiconductors with respect to the water redox potential. After introduction of those small band gap oxides, the increased light absorption and photocatalytic efficiency were enabled by the utilization of visible light.

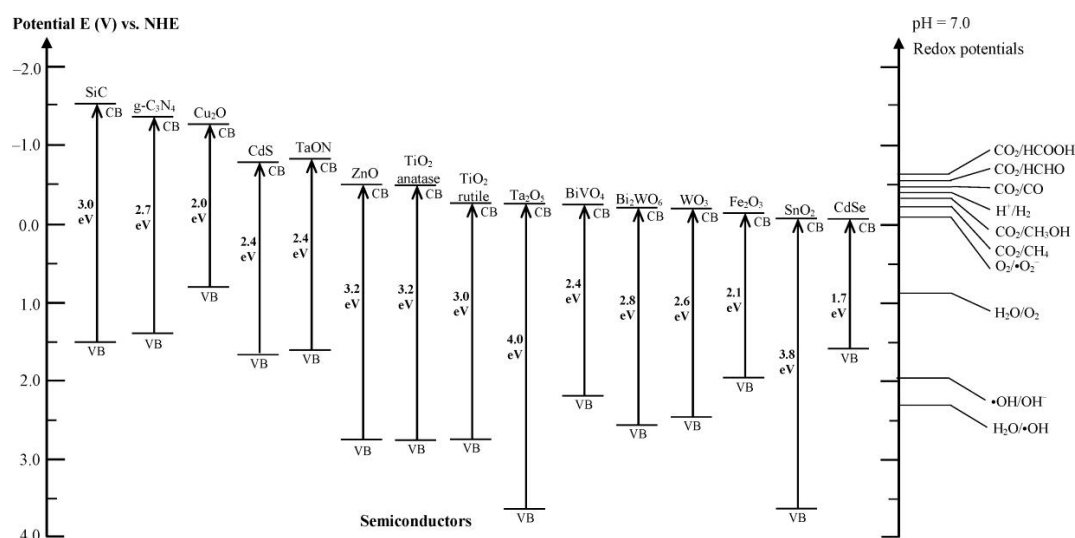


**Figure 2.** Band edge positions of various semiconductors with respect to the water redox potentials. Reprinted with permission from [3]. Copyright 2016, American Chemical Society.

Another solution for overcoming the limitation of the light absorption is the application of localized surface plasmon resonance (LSPR) in metal nanoparticles (NPs) [36,37]. LSPR represents the oscillation of electrons in the metal NPs in response to the incident light, or electromagnetic waves. The physical phenomena for the LSPR-induced enhancement effects include: (1) the formation of the localized electric field and (2) the enhanced light absorption by the oscillation of the surface plasmon in the metal, which made is response to the incident light, and thereby, (3) the enhanced charge carrier generation [16]. Many researchers have reported the application of metal NPs into their PEC devices, since a peak resonant wavelength can be controlled in the visible region through adjusting metal elements, size, and shape [9,16,17,23,36–40]. This strategy is so called “plasmonic photocatalysis”. In the field of plasmonic photocatalysis, Au [9,17,20,23,32,41,42] and Ag [16,43] are the most frequently used metal species. Au and Ag NPs have been introduced to oxide semiconductors such as  $\text{BiVO}_4$  [9,16,17,20,23],  $\text{TiO}_2$  [41–43], and  $\text{Fe}_2\text{O}_3$  [32]. In addition to the monometallic NPs, the multi-metallic NPs of PtAuCu alloys have been recently discovered as an effective hydrogen evolution catalyst [44]. Therefore, it is reasonable to expect that the investigation of multi-metallic NPs on the plasmonic photocatalysis will be performed in the near future.

Recently, Lee et al. reported the  $\text{BiVO}_4$  photoanode with shape-controlled Au NPs [23]. The shape-dependent LSPR effect was observed in the device, as shown in Figure 3a,b. The hemispherical Au NPs were deposited by an e-beam evaporator directly on the  $\text{BiVO}_4$  film, whereas the octahedral Au NPs were synthesized using seed-mediated growth method followed by attachment on the  $\text{BiVO}_4$ . The authors performed a finite-difference time-domain (FDTD) simulation to represent the spatial distribution of the LSPR-induced electric fields (LSPR-EFs) near the Au NPs (Figure 3c–h). The results showed that the octahedral Au NP shows higher LSPR-EFs, especially at sharp edges of the Au NP, than that of the hemispherical one. The  $\text{BiVO}_4$  with the octahedral Au NPs showed the best PEC performance (Figure 3i) and the enhancement could be explained as above. Moreover, the Mott-Schottky plot under dark conditions (Figure 3j) showed a lower flat band potential for the  $\text{BiVO}_4$  with octahedral Au NPs than that of bare  $\text{BiVO}_4$ , which implies a more favorable band position for the PEC water splitting. Therefore, the improvement of PEC performance was attributed to the LSPR-induced enhanced light absorption by the plasmonic Au NPs on the  $\text{BiVO}_4$  film.

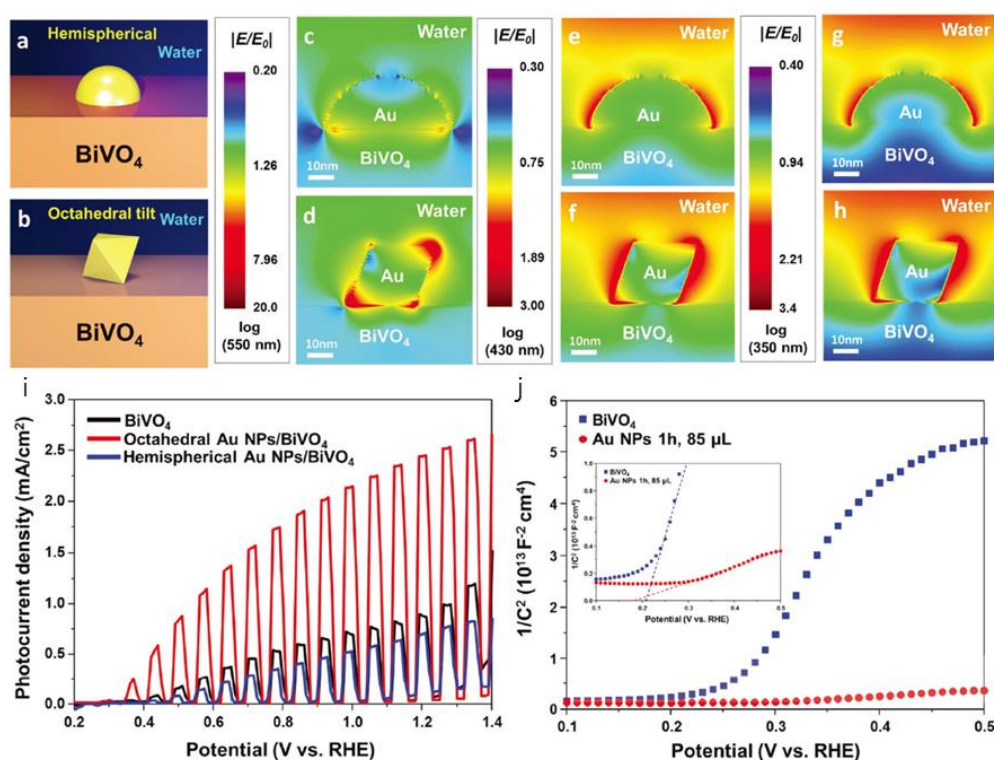


**Figure 3.** Finite-difference time-domain simulation results of  $\text{BiVO}_4$  with (a) hemispherical Au NP and (b) octahedral Au NP. The simulations are performed under wavelengths of (c,d) 550 nm, (e,f) 430 nm, (g,h) 350 nm. (i) PEC performances of the samples. (j) Mott-Schottky plot of bare  $\text{BiVO}_4$  and  $\text{BiVO}_4$  with octahedral Au NPs under dark conditions (Frequency: 1 kHz, amplitude: 10 mV). Reprinted with permission from [23]. Copyright 2017, John Wiley and Sons.

Zhang et al. investigated the size-dependent LSPR effect of Au NPs on the  $\text{BiVO}_4$  film. They prepared Au NPs with diameters of 10, 20, 30, 40, 60, and 80 nm. All samples with Au NPs showed enhanced PEC performance over the pristine  $\text{BiVO}_4$  film, and 20 and 30 nm diameters exhibited the highest photocurrent densities. In order to elucidate the reason for the enhancement, they performed FDTD simulation so that the LSPR-EFs in the different sizes of the Au NPs were simulated. The results indicated that the electric field enhancement was increased an increase in the diameter of Au NP. Therefore, photoexcited holes in the  $\text{BiVO}_4$  could diffuse to the surface of  $\text{BiVO}_4$  film and participate in the water redox reaction. Meanwhile, the visible light absorption was also improved by the presence of the Au NPs. Light absorption enhancement exhibited the maximum at around 530 nm, regardless of the size of the Au

NPs. Thus, it can be inferred that the enhancement of PEC performance is attributed to the improved visible light absorption and effective carrier separation by the LSPR-EFs at the interface.

## 2.2. Separation and Transport of Charge Carrier

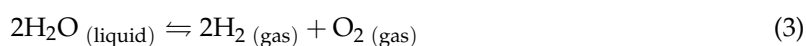
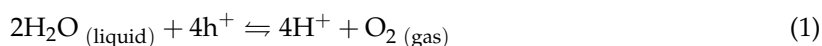
The photoexcited charge carriers in the photoelectrode need to move to active sites for participation in the water redox reaction. In order to efficiently split the water molecules and produce the hydrogen gas, these charge carriers avoid recombination before they reach the active sites. One promising solution is the creation internal built-in potential which forces the charge carriers to move to the surface. The internal potential can be created by forming heterojunctions with different oxides, doping of foreign elements, or introducing a metal onto the semiconductor [45]. The formation of heterojunction has been accepted as one of the most promising ways for the practical photocatalysts because of its effectiveness in separating electron-hole pairs. Therefore, much research has been reported on the enhancement of PEC performance in this manner.

Grigioni and co-workers reported on wavelength-dependent charge carrier separation in the WO<sub>3</sub>-BiVO<sub>4</sub> heterostructure film [11]. Although many research results have suggested the improved carrier separation of the WO<sub>3</sub>-BiVO<sub>4</sub> heterostructure, an understanding of the underlying dynamics is still elusive. Thus, they investigated the lifetime of photoexcited holes in the WO<sub>3</sub>-BiVO<sub>4</sub> heterojunction by femtosecond transient absorption (TA) measurement with tunable pump wavelength. The results showed that the charge carrier transfer between the WO<sub>3</sub> and the BiVO<sub>4</sub> depends on the wavelength of irradiation. At a wavelength that is longer than the absorption edge of the WO<sub>3</sub>, the lifetime of photoexcited holes in the WO<sub>3</sub>-BiVO<sub>4</sub> was longer than that of the single BiVO<sub>4</sub> since the holes were effectively transferred into the WO<sub>3</sub>. However, when the wavelength was tuned across the absorption edge of the WO<sub>3</sub>, which were 460 nm and 387 nm in this report, the lifetime of holes in the WO<sub>3</sub>-BiVO<sub>4</sub> were decreased. The authors attributed the results to the increased electron-hole recombination at the interface between the BiVO<sub>4</sub> and the WO<sub>3</sub>. That is, the electron excitation from valence band of the WO<sub>3</sub> at such conditions leads to the recombination of electrons from the WO<sub>3</sub>, and holes in the BiVO<sub>4</sub>. This tells us that another route for the recombination in the heterojunction of photocatalysts can negatively affect the whole PEC process, and thus, we need to carefully design the heterostructured PEC devices for efficient solar water splitting.

The doping of the photocatalysts also has been explored as one of the promising solutions. Recently, Abdi et al. investigated the Ca-doped BiVO<sub>4</sub> system (Ca:BiVO<sub>4</sub>) [24]. The authors deposited the Ca-doped BiVO<sub>4</sub> thin films by spray pyrolysis. During the deposition process, interestingly, spontaneous out-diffusion of Ca took place, which was resulted in gradual band bending through the film. Then, internal bend banding in the Ca:BiVO<sub>4</sub> promoted the carrier separation in the bulk of film, since the out-diffusion of Ca occurred over the entire region. Moreover, the higher catalytic activity of the Ca-rich BiVO<sub>4</sub> surface for water splitting contributed the enhanced performance. In the past, they had reported on the gradient W-doped BiVO<sub>4</sub> (W:BiVO<sub>4</sub>) [6]. In that report, they deposited a 10-step gradient-doped W:BiVO<sub>4</sub>. As a result, the photocurrent was enhanced by about 60%, in comparison with that of the homogeneously W-doped BiVO<sub>4</sub>. Both results reported by the authors show that the poor carrier separation efficiency of the BiVO<sub>4</sub> can be overcome by forming a multi-step doping method, thus creating effective built-in band bending. It is notable that the proposed strategy may be generally applicable to various oxide photoelectrode materials.

## 2.3. Kinetics of Water Redox Reactions

The basic water splitting reactions may be expressed as following water redox reactions:



Reaction (1) represents the water oxidation half reaction at the anode, also called the oxygen evolution reaction (OER). In the same manner, the water reduction half reaction in reaction (2) is called the hydrogen evolution reaction (HER). The overall water redox reaction in reaction (3) shows that the water is split into hydrogen and oxygen gases. In the redox reaction, the bottleneck lies in the OER (reaction (1)) since the delicate bond rearrangements of the two water molecules should take place to transform into the oxygen gas instead of its high-energy intermediates [46]. Thus, it induces the slow water oxidation kinetics, and unused holes are accumulated on the electrode surface. The accumulation of photoexcited holes is known as the reason for the photocorrosion of  $\text{BiVO}_4$ , which reduces long-term stability as the photoanode [47]. In order to solve the problem, some solutions have been introduced, such as increasing the density of surface active sites or combining them with oxygen evolution co-catalysts (OECs). Recently, our group reported on the deposition of a high quality polycrystalline  $\text{BiVO}_4$  photoanode with a controllable surface area [10]. The  $\text{BiVO}_4$  film was grown by pulsed laser deposition (PLD), and the surface area of film was optimized by controlling process temperatures during growth of the  $\text{BiVO}_4$ . As shown in Figure 4a–c, the morphology of the  $\text{BiVO}_4$  film could be controlled, since the growth condition satisfies a 3-dimensional island growth mode (the Volmer-Weber growth). At a low temperature of 230 °C, diffusion of Bi was suppressed and it resulted in the small  $\text{BiVO}_4$  grains being separated by voids (Figure 4a). When the temperature was increased to 330 °C and 430 °C, the voids disappeared by intergrain diffusion, and eventually, the coalescence of  $\text{BiVO}_4$  grain took place (Figure 4b,c). Therefore, the surface area of  $\text{BiVO}_4$  film decreased and it affected the PEC performance. As shown in Figure 4d–f, as the process temperature decreased to 230 °C, the interfacial area between the  $\text{BiVO}_4$  grains and the electrolyte increased. Moreover in the case, the photoexcited electrons in the  $\text{BiVO}_4$  grains were more effectively transferred to the bottom FTO electrode without recombination in bulk. Therefore, the PEC performance of the  $\text{BiVO}_4$  grown at 230 °C exhibited the highest current density of  $\sim 3.0 \text{ mA/cm}^2$  at 1.23  $V_{\text{RHE}}$ , and the incident photon-to-current efficiency (IPCE) approaching 35% at the wavelength of 400 nm (Figure 4g,i). To elucidate the effect of the differences in light absorption, UV-vis-NIR absorption spectra were measured (Figure 4h). Note that the films grown at 230 and 330 °C clearly showed the visible light absorption. Consequently, it was implied that the improved PEC performance of the film grown at 230 °C was dominated by the increased surface area itself. The results of this study were quite interesting, since the excellent PEC performance of  $\sim 3.0 \text{ mA/cm}^2$  was exhibited from a single layer of the  $\text{BiVO}_4$ .

Along with the surface area control, the deposition of the OECs on the surface of photoelectrode has been one of the promising approaches for boosting the OER and increasing the stability of  $\text{BiVO}_4$  [21]. So far, the OECs have been deposited mostly by electrodeposition [48]. However, recently, Tang et al. introduced another method for OEC synthesis [49]. They investigated a strategy to deactivate the surface trapping states between  $\text{BiVO}_4$  and the OEC of  $\text{CoOOH}$  by synthesizing ultrathin  $\text{CoOOH}$  layers on the  $\text{BiVO}_4$  surface. In order to synthesize the ultrathin OECs on the  $\text{BiVO}_4$  surface, they used a hydrothermal method for firstly synthesizing the  $\text{Co(OH)}_2$  nanosheet. The obtained  $\text{Co(OH)}_2$  nanosheets were then dispersed into ethyl alcohol, followed by spin coating onto the prepared  $\text{BiVO}_4$  sample. Owing to the hydrothermal process for  $\text{Co(OH)}_2$  synthesis, the ultrathin OEC nanosheets were synthesized and the coverage of the multilayered  $\text{CoOOH}$  on the 3D coral-like  $\text{BiVO}_4$  surface were possible to produce. After heating, covalent-bonding between the  $\text{CoOOH}$  and the  $\text{BiVO}_4$  took place, which was crucial for deactivating the surface trapping states and promoting the charge separation. Consequently, the 3D coral-like  $\text{BiVO}_4$  with the ultrathin  $\text{CoOOH}$  OEC showed a larger photovoltage of 0.28 V, and a significant negative shift of onset potential than that of the pristine  $\text{BiVO}_4$  sample. The authors claimed that the great reduction in the number of surface trapping states could effectively facilitate the separation efficiency of photocarriers, even at a low-bias potential. Therefore, it could be inferred that more efficient and practical PEC water splitting devices could be realized by designing not only the photoelectrode itself, but also the effective configuration of the OECs on it.

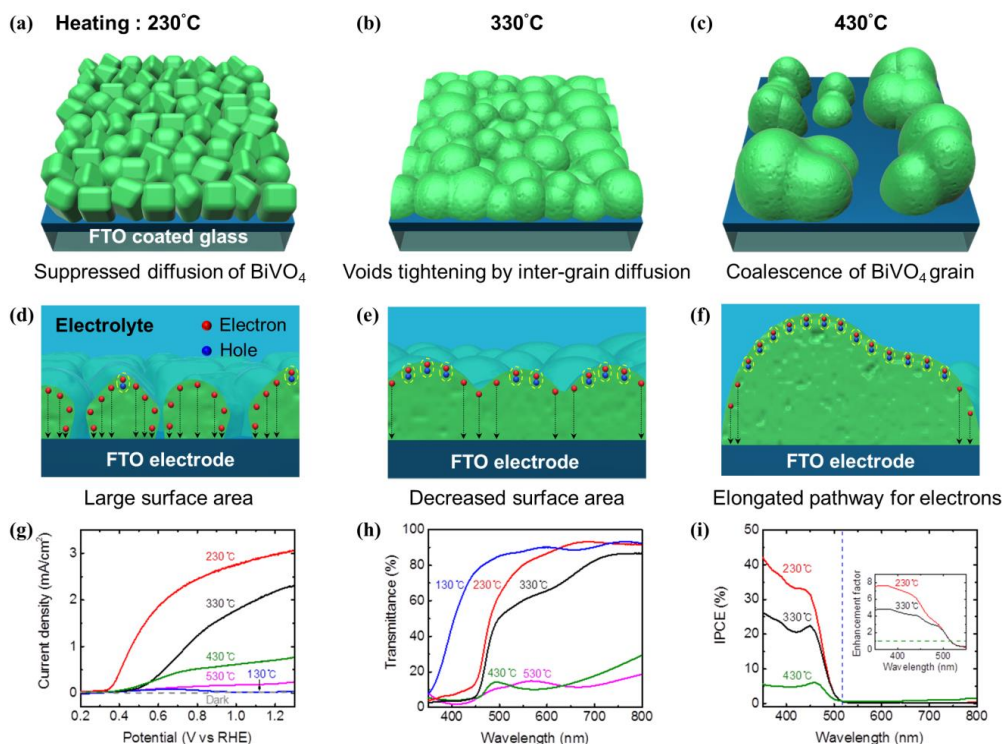


**Figure 4.** Schematic representation of surface area-controlled BiVO<sub>4</sub> film deposited by pulsed laser deposition. Microstructural changes and charge collection abilities of BiVO<sub>4</sub> film deposited at (a,d) 230 °C, (b,e) 330 °C, (c,f) 430 °C. (g) PEC performances, (h) UV-vis transmission spectra, and (i) incident photon-to-current efficiency (IPCE) of the samples. Reprinted with permission from [10]. Copyright 2017, American Chemical Society.

### 3. Challenging PEC Device Designs toward Practical Solar Water Splitting

The step processes of PEC water splitting and the strategies for improving each step process are discussed so far. In this section, we will introduce the state-of-the-art of the PEC device designs and the fabrication techniques, including the application of facet engineering and the development of a ferroelectric coupled PEC device. These up-to-date research fields are still in their infancy, so we would like to refer to some representative works in years of recent development. The realization of such device designs is challenging, especially since it requires carefully controlled material growth techniques to expose favorably oriented crystal facets on the surface. Moreover, the application of ferroelectric into the PEC water splitting requires rigid and stable ferroelectric performance, with properties that can be made through elaborate fabrication methods, such as vacuum deposition of pulsed laser deposition (PLD) [33,35]. As a physical vapor deposition technique, PLD is well-known, as its advantages for its deposition of pure and highly crystalline thin film [50,51]. Owing to the aforementioned advantages, epitaxial thin films for various applications have been grown by the PLD and there are numerous designs of thin films and heterostructures [52]. Recently, there have been many attempts to investigate the PEC water splitting performance of epitaxial thin film photocatalysts for better understanding on the material properties. The remaining part of the section will deal with some recent progress on these challenging and fascinating research fields.

#### 3.1. Application of Facet Engineering in PEC Water Splitting

Many theoretical predictions based on computational methods shows that intrinsic anisotropic material properties such as electronic and optical properties in semiconductors should be understood for better explanation on the enhancement mechanism and realization of practical PEC devices. For instance, the intrinsic carrier transport properties and optical properties, depending on the

crystallographic orientations of monoclinic-scheelite  $\text{BiVO}_4$ , have been calculated using density functional theory (DFT) [53,54]. The calculation results show that the mobility of charge carriers is different depending on the  $\text{BiVO}_4$  crystal axis [54]. In detail, the mobility of electrons along [010] is 5 times higher than that of the [110] direction where  $a = 5.195 \text{ \AA}$ ,  $b = 11.701 \text{ \AA}$ ,  $c = 5.094 \text{ \AA}$ . In the same manner, however, the mobility of holes along [110] is two times higher than that of the [010] direction. Furthermore, it has been also known that the optical properties such as refractive indices and light absorption are different, so that preferentially oriented crystals can have spectral selectivity compared with the corresponding bulk crystal [53]. Therefore, it is implied that the devices with preferentially oriented crystal facets are needed since optimization between the carrier transport properties and light absorption of photoelectrodes can be achieved using such systems. There are some experiments on these considerations. Mostly, investigations have been performed for various semiconductors including  $\text{BiVO}_4$  [18,20],  $\text{TiO}_2$  [55], and  $\text{Fe}_2\text{O}_3$  [28] in the form of powder. In order to investigate the facet-dependent PEC activity, those investigations showed photoreduction of Au or Ag compound on certain facet of the semiconductors. As a result, distinctive morphological changes, which were owing to the reduction of Au or Ag compound by photoexcited electrons at certain facets, could be observed by SEM images of each sample. However in those experimental circumstances, further understandings on PEC processes such as the carrier separation efficiency and the water redox kinetics, are limited. So far, a few research groups have reported on the fabrication of the preferentially oriented photoelectrode thin films, and have demonstrated the facet engineering that can show the relation between the facets of the semiconductor and the PEC water splitting activity. Han et al. deposited [001] preferentially oriented polycrystalline  $\text{BiVO}_4$  (p-BVO) thin films (where  $a = 5.1935 \text{ \AA}$ ,  $b = 5.0898 \text{ \AA}$ ,  $c = 11.6972 \text{ \AA}$ ) on F-doped  $\text{SnO}_2$  (FTO) glass substrates by PLD [15]. For comparison, they also synthesized randomly oriented  $\text{BiVO}_4$  (r-BVO) by a sol-gel method. The synthesized films showed that about 41% of the  $\text{BiVO}_4$  grains were [001] oriented in the p-BVO while this was only ~3% for the r-BVO. Thus, a schematic image for the p-BVO and the r-BVO could be represented, as shown in Figure 5a. The PEC performance of both samples clearly showed that the photocurrent density of the p-BVO reached  $\sim 3.9 \text{ mA/cm}^2$  at  $1.23 V_{\text{RHE}}$  which was about 16 times higher than that of the r-BVO (Figure 5b–d). A higher IPCE of the p-BVO (Figure 5d) could be attributed to the efficient charge separation (Figure 5f) and transport (Figure 5g) of the p-BVO in comparison with the r-BVO, since almost the same light absorption spectra were observed (Figure 5e). The results obviously indicated that the increased carrier transfer and the transport efficiency contributed to the improved PEC performance of the p-BVO. The electrochemical impedance spectroscopy (EIS) measurement supported the results by showing the smaller bulk and interface resistances of the p-BVO (Figure 5h).

However, in order to more deeply understand the intrinsic carrier transport properties depending on the crystallographic orientations and facets of the monoclinic-scheelite  $\text{BiVO}_4$ , it is necessary to study the establishment of epitaxial single crystalline thin films. In general, the establishment of epitaxial thin film photoelectrode has been widely recognized to maximize the potential of photoelectrode materials in pursuit of a further breakthrough by exploring its fundamental properties. For that reason, recently, various research on the growth of the epitaxial  $\text{BiVO}_4$  have been reported, to explore its fundamental properties for PEC water splitting [13,19,56–63]. Based on many theoretical predictions, the research related to the growth of the epitaxial monoclinic  $\text{BiVO}_4$  ( $a = 5.1956 \text{ \AA}$ ,  $b = 5.0935 \text{ \AA}$ ,  $c = 11.6972 \text{ \AA}$ ,  $\beta = 90.387^\circ$ ) films have been focused on growth along the  $c$ -axis. The growth of epitaxial  $\text{BiVO}_4$  (001) thin films was firstly achieved on a yttria-stabilized zirconia (YSZ,  $a = 5.145 \text{ \AA}$ ) substrate by molecular beam epitaxy [56]. However, the PEC properties for the epitaxial  $\text{BiVO}_4$  (001) thin films could have not measured due to the absence of conductive electrode materials. On the other hand, Van et al. fabricated the epitaxial  $\text{BiVO}_4$  (001) thin films by the PLD, and the photocathodic properties for the epitaxial  $\text{BiVO}_4$  (001) thin films were observed by introducing  $\text{SrRuO}_3$  as the bottom electrode [58]. In addition to epitaxial monolayer thin films, many studies have been reported on epitaxial heterojunction thin films. Our group recently reported that the self-assembled  $\text{BiVO}_4$ - $\text{WO}_3$  heterostructured thin films could be grown epitaxially in the  $c$ -axis orientation to investigate the charge interaction between the

BiVO<sub>4</sub> and the WO<sub>3</sub> [59]. The growth of epitaxial BiVO<sub>4</sub> (001) thin films also could be achieved on the SrTiO<sub>3</sub> (001) (STO,  $a = 3.905 \text{ \AA}$ ) substrate by the insertion of the WO<sub>3</sub> as template layer, which could reduce the lattice mismatch between the BiVO<sub>4</sub> and the STO [13]. In addition, Zhang et al. reported on the improved PEC performance of the epitaxial BiVO<sub>4</sub> (001) thin film by inserting lutetium oxide (Lu<sub>2</sub>O<sub>3</sub>) as a hole blocking layer [60].

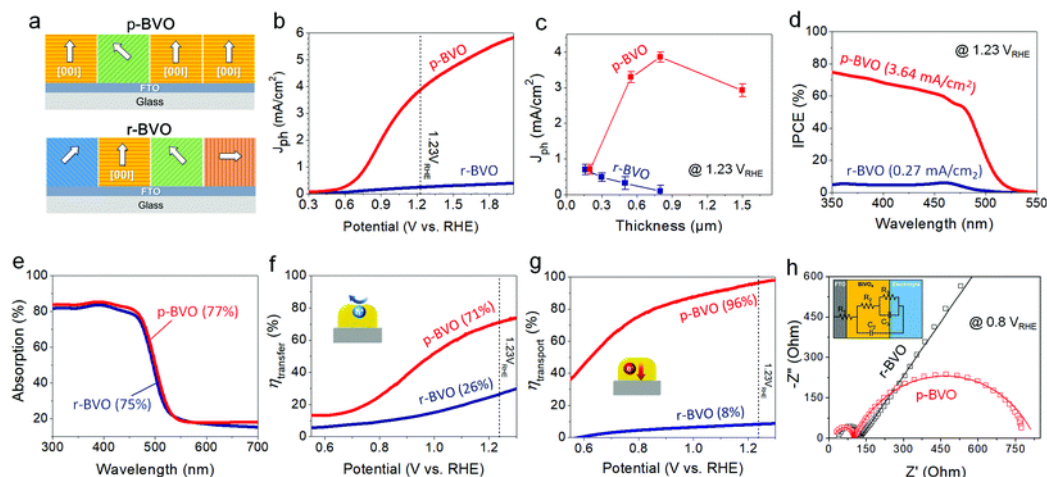


**Figure 5.** (a) Schematic representation of crystallographic orientations of preferentially oriented polycrystalline BiVO<sub>4</sub> (p-BVO) and randomly oriented BiVO<sub>4</sub> (r-BVO). (b) PEC performances. (c) Thickness dependence of photocurrent density. (d) IPCE. (e) Light absorption. (f) Charge transfer efficiency. (g) Charge transport efficiency. (h) Electrochemical impedance spectroscopy (EIS) spectra measured at 0.8 V<sub>RHE</sub> under simulated light irradiation (100 mW/cm<sup>2</sup>). Reprinted with permission from [15]. Copyright 2018, Royal Society of Chemistry.

Although the above-mentioned studies have well demonstrated on the growth of epitaxial BiVO<sub>4</sub> (001), further identification of the theoretical predictions that the electrical conductivity of the BiVO<sub>4</sub> is greater along the *ab*-plane than along the *c*-axis requires more challenging investigations and techniques [62,63]. The anisotropic transport property of the BiVO<sub>4</sub> can be explained in terms of the crystalline structure, which is that charge carrier transport along the *c*-axis is only generated by nearest-neighbor hopping, while along the *ab*-plane it can be generated by both nearest-neighbor hopping and next-nearest-neighbor hopping. Therefore, the difference causes the enhanced hopping in the *ab*-plane. Most recently, based on the anisotropic electrical conductivity of the BiVO<sub>4</sub>, the anisotropic charge transport efficiency of the BiVO<sub>4</sub> has been investigated by fabricating the epitaxial oxide thin films with different crystallographic orientations for the PEC water splitting [19]. In that report, the epitaxial BiVO<sub>4</sub> (001) thin films were fabricated on the YSZ (001) substrate as reported in the previous studies, while the epitaxial BiVO<sub>4</sub> (010) thin films were firstly grown on the STO (001) substrate by the domain match epitaxy (DME). Interestingly, the photocurrent density of the epitaxial BiVO<sub>4</sub> (010) (2.29 mA/cm<sup>2</sup>) showed significantly enhanced values in comparison with that of the epitaxial BiVO<sub>4</sub> (001) (0.74 mA/cm<sup>2</sup>) due to the improvement of the charge transport efficiency as shown in Figure 6a. The EIS spectra of the epitaxial BiVO<sub>4</sub> with different crystallographic orientations revealed that a smaller semicircle in the epitaxial BiVO<sub>4</sub> (010) was observed due to the high photoactivity, and the better kinetic charge transfer (Figure 6b). The wavelength-dependent properties observed by the IPCE also showed that it was significantly enhanced in the epitaxial BiVO<sub>4</sub> (010) than that of the epitaxial BiVO<sub>4</sub> (001) (Figure 6c). Consequently, it could be understood that the in-depth understanding on effect of specific crystallographic orientations in the design of the metal oxide thin film photoelectrodes would be highly beneficial for the further improvement of performances, and a deeper understanding of PEC water splitting.

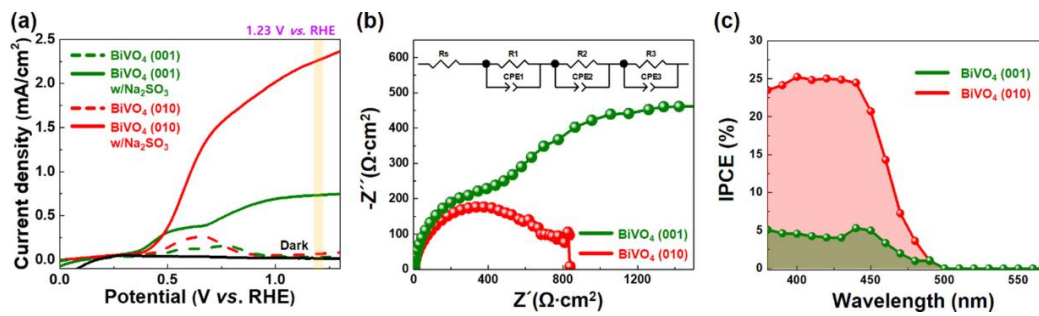


**Figure 6.** (a) PEC performances of 100 nm-thick epitaxial  $\text{BiVO}_4$  films with different crystallographic orientations. The electrolyte of 0.5 M  $\text{Na}_2\text{SO}_4$  aqueous solutions in the presence or absence of 0.5 M  $\text{Na}_2\text{SO}_3$  was used for the measurement. (b) EIS spectra and (c) IPCE of the  $\text{BiVO}_4$  with different crystallographic orientations. Inset of (b) shows the equivalent circuit for the data. Reprinted with permission from [19]. Copyright 2018, American Chemical Society.

### 3.2. Development of Ferroelectric Coupled PEC Device

In order to efficiently convert solar energy into electrical or chemical energy, the charge carrier separation and collection has generally been considered as one of the most decisive factors. Also, it is well known that the internal electric field developed in conventional p–n junctions enables efficient charge separation and collection. Hence, attempts to utilize the unusual photovoltaic effect of the ferroelectric oxides have been widely reported. The studies have shown that the spontaneous polarization of the ferroelectric oxides, which creates an internal electric field, provides significant improvements in the charge carrier separation and collection. Herein, the correlation between the spontaneous polarization and the internal electric field can be explained as follows. The high built-in-potential at the interface is determined by quantifying the polarization effect, which can be indicated as the potential height of ferroelectric band bending ( $P\delta/\epsilon$ , Equation (4)). Additionally, the electric field at the interface can be determined by Equation (5) [64].

$$V_{bi}' = V_{bi} \pm \frac{P}{\epsilon} \delta \quad (4)$$

$$E = \sqrt{\frac{2qN_{eff}(V + V_{bi}')}{\epsilon}} \pm \frac{P}{\epsilon} \quad (5)$$

where  $V_{bi}'$  is the built-in potential at the interface,  $V_{bi}$  is the built-in potential,  $P$  is the polarization of ferroelectrics,  $\epsilon$  is the dielectric constant,  $\delta$  is the distance between the polarization charge and the interface with the electrode,  $E$  is the electric field at the interface,  $q$  is the electric charge, and  $N_{eff}$  is the effective charge density. Note that the spontaneous polarization and the internal electric field are linearly aligned. Recently, many studies have been widely conducted to apply this unique property of the ferroelectric materials to PEC water splitting. However, in spite of the advantageous photovoltaic effect, most ferroelectric materials, including  $\text{BaTiO}_3$ ,  $\text{PbTiO}_3$ , and  $\text{Pb}(\text{Zr}, \text{Ti})\text{O}_3$  typically have the wide bandgap that absorbs only a short range of the visible spectrum [65]. Fortunately, among the ferroelectric materials, the  $\text{BiFeO}_3$  have a relatively narrow bandgap in the range 2.2–2.7 eV [66,67]. For that reason, various studies on the ferroelectric  $\text{BiFeO}_3$  photoelectrodes have been reported for PEC water splitting [35,68–73]. Recently, our group reported that the effect of applying ferroelectric  $\text{BiFeO}_3$  thin films to PEC water splitting, which could be systematically summarized as shown in Figure 7 [35]. As described in Figure 7a–c, the schematic shows the energy band diagram of the  $\text{BiFeO}_3$  thin film photoanodes in the PEC water splitting system to help with understanding on the effect of ferroelectric switching with different polarization states. In the no-polarization state, each photoexcited carriers are separated inefficiently on both sides of the photoanode without the energy band bending (Figure 7a). However, the downward ferroelectric switching of  $\text{BiFeO}_3$  induces negative (positive) bound charges toward the electrolyte/photoanode (photoanode/bottom electrode)

interface (Figure 7b). As a result, each band bending significantly enhances PEC performances. On the other hand, the high built-in-potential by the ferroelectric polarization causes upward (downward) band bending toward the electrolyte/photoanode (photoanode/bottom electrode) interface. In this case that the upward ferroelectric switching of the BiFeO<sub>3</sub> is induced, each band bending operates as the barrier for photoexcited carriers, and this deteriorates PEC performances (Figure 7c). In addition, interestingly, BiFeO<sub>3</sub> has been widely reported to have different polarization values with different crystallographic orientations, as shown in Figure 7d [74–78]. The different ferroelectric polarization values of the BiFeO<sub>3</sub>, which depend on different crystallographic orientations, induce the differences in the energy band bending height. Figure 7e indicates the difference in the energy band bending height induced by the different spontaneous polarization values in the downward polarization state. Especially, (111)<sub>pc</sub>-oriented BiFeO<sub>3</sub> has the highest energy band bending height because of its highest spontaneous polarization value among all crystallographic orientations. In conclusion, the most efficient charge separation and collection of the photogenerated carriers can be obtained in the (111)<sub>pc</sub> BiFeO<sub>3</sub> photoanode.

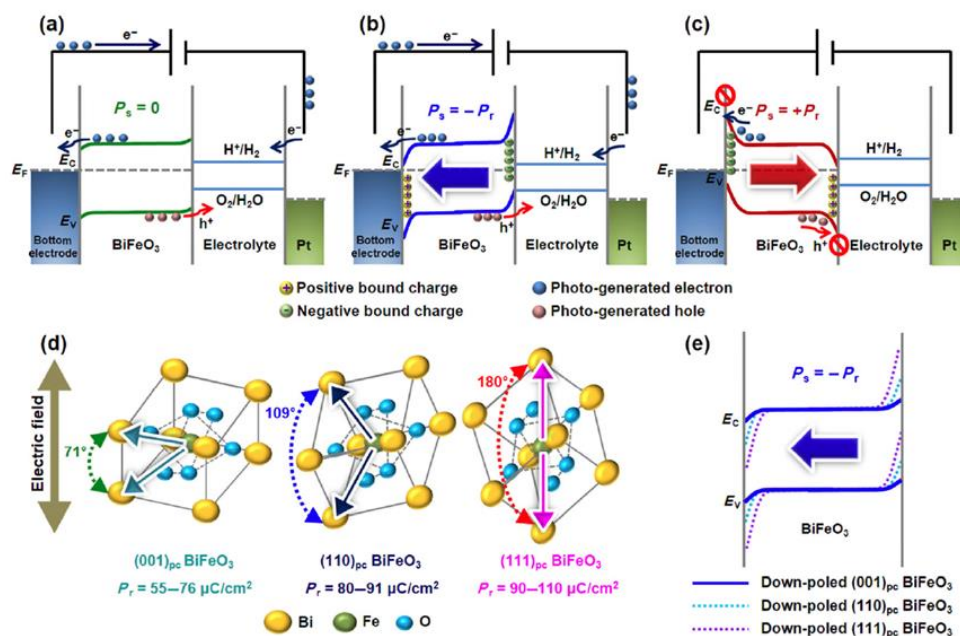


**Figure 7.** Schematic representations of the built-in polarization field in (a) no polarization state, (b) downward polarization state, and (c) upward polarization state of ferroelectric BiFeO<sub>3</sub> thin films. (d) Different polarization values of BiFeO<sub>3</sub> with different crystallographic orientations. (e) Polarization direction of the BiFeO<sub>3</sub> in different crystallographic orientations. Reprinted with permission from [35]. Copyright 2018, Tsinghua University Press and Springer-Verlag GmbH Germany.

There are many limitations inherent in the ferroelectric materials in terms of the light absorption and the photoactivity when using ferroelectric materials alone as PEC water splitting photoelectrodes. Thus, in recent years, the ferroelectric materials have not been used as a single material for the PEC water splitting, but as a part of the heterojunction structures to harness the ferroelectric energy band bending. For instance, Yang et al. synthesized the ferroelectric BaTiO<sub>3</sub>/TiO<sub>2</sub> heterojunction structure, which exhibited the improved PEC performances as a result of the enhanced charge separation efficiency induced by the ferroelectric polarization of BaTiO<sub>3</sub> [79]. In addition, Xie et al. reported the PEC performance of the ferroelectric BiFeO<sub>3</sub>/BiVO<sub>4</sub> composite photoanode fabricated by the chemical solution deposition [34]. The result showed that the photoanodic property of the ferroelectric BiFeO<sub>3</sub>/BiVO<sub>4</sub> heterostructure film was significantly improved by the effect of the surface passivation and the reduced charge recombination by the BiFeO<sub>3</sub>. To date, it is known that the built-in band bending

induced by the spontaneous polarization of the ferroelectric materials enables the improved charge separation. Because the application of ferroelectric materials into PEC water splitting has plentiful of undiscovered strategies that are yet to be explored, it is expected to be intensively investigated.

#### 4. Conclusions and Future Outlook

Energy harvesting technology from the unlimited source of solar radiation has been considered as a sustainable solution for the global energy challenge. In that respect, the solar-driven water splitting technology has greatly progressed so far, since hydrogen as a product of water splitting reaction is expected to support future societies. Here, we reviewed the enhancement strategies, and recent progress on the device designs toward the efficient and practical PEC solar water splitting. In decades of research, many researchers have endeavored to discover small band gap semiconductors, and this has resulted in the development of  $\text{BiVO}_4$ ,  $\text{Fe}_2\text{O}_3$  etc. Introduction of those semiconductors into the photoelectrode have brought the utilization of visible light, which results in increased photocatalytic efficiency. However, there are still problems remaining, such as the poor charge separation in the bulk and the slow oxidation kinetics. Recently, various efforts are being investigated, including the strategies of fabricating heterostructures, loading plasmonic NPs, gradient-doping of foreign elements, and synthesizing OECs on the surface. Due to the above-mentioned efforts, more efficient charge separation efficiency and faster kinetics of oxidation have been achieved, and this enables a deep understanding of PEC water splitting. Moreover, the application of plasmonic NPs into PEC water splitting has made it possible to develop visible-light-responsive photoelectrodes consisting of large band gap oxides. Based on these achievements, it is expected that further improvements of the plasmonic photocatalysts will be available by designing plasmonic NPs with various shapes, structures, and compositions.

Most recently, in order to achieve further improvement, very interesting and challenging attempts are being explored. One is so-called facet engineering which requires delicate material growth techniques to expose certain crystal facets on the surface of photoelectrodes. By DFT calculations, it is known that the intrinsic carrier transport properties and the light absorption abilities are different depending on the crystallographic orientations of semiconductors. Therefore, a PEC device with preferentially oriented crystal facets on its surface is crucial for achieving optimization between the carrier transport, the light absorption efficiency, and the water oxidation kinetics. The other one is a ferroelectric coupled PEC device. To date, the positive effect of the built-in potential induced by the spontaneous polarization of the ferroelectrics on charge separation has been reported. However, this state-of-the-art PEC device design is still in its infancy. Although the fabrication of ferroelectrics requires the elaborate deposition process, well known facts on ferroelectrics, such as the different polarization values depending on the different crystallographic orientations, imply that there are numerous of undiscovered fascinating strategies.

The various enhancement strategies and the device designs are summarized in this review. We believe that the practical PEC water splitting can be achieved by combining two or more introduced strategies and designs. Especially, the combination of the OECs and the facet engineering or the ferroelectric coupled PEC devices seem more promising and fascinating. In addition, the cost-effectiveness and the long-term stability should be considered for the commercialization of PEC water splitting technology. In that respect, the use of inexpensive materials, for example, semiconductors including  $\text{BiVO}_4$ ,  $\text{BiFeO}_3$ , and  $\text{Fe}_2\text{O}_3$ , and OECs of  $\text{NiOOH}$ ,  $\text{FeOOH}$ ,  $\text{CoOOH}$  etc. should be taken into account for future development.

**Author Contributions:** S.L. supervised the overall project and S.Y.J., J.S. and S.L. co-wrote the manuscript.

**Funding:** This research was funded by [Ministry of Education-Korea] grant number [NRF- 2016R1D1A1B03931748] and [Ministry of Science and ICT-Korea] grant number [NRF- 2017M3D1A1040828].

**Conflicts of Interest:** The authors declare no conflict of interest.

## References

1. Turner, J.A. Sustainable hydrogen production. *Science* **2004**, *305*, 972–974. [[CrossRef](#)] [[PubMed](#)]
2. Jiang, C.; Moniz, S.J.; Wang, A.; Zhang, T.; Tang, J. Photoelectrochemical devices for solar water splitting—materials and challenges. *Chem. Soc. Rev.* **2017**, *46*, 4645–4660. [[CrossRef](#)] [[PubMed](#)]
3. Ong, W.-J.; Tan, L.-L.; Ng, Y.H.; Yong, S.-T.; Chai, S.-P. Graphitic carbon nitride (g-C<sub>3</sub>N<sub>4</sub>)-based photocatalysts for artificial photosynthesis and environmental remediation: Are we a step closer to achieving sustainability? *Chem. Rev.* **2016**, *116*, 7159–7329. [[CrossRef](#)] [[PubMed](#)]
4. Fujishima, A.; Honda, K. Electrochemical photolysis of water at a semiconductor electrode. *Nature* **1972**, *238*, 37–38. [[CrossRef](#)] [[PubMed](#)]
5. Abdi, F.F.; Firet, N.; van de Krol, R. Efficient BiVO<sub>4</sub> thin film photoanodes modified with cobalt phosphate catalyst and W-doping. *ChemCatChem* **2013**, *5*, 490–496. [[CrossRef](#)]
6. Abdi, F.F.; Han, L.; Smets, A.H.; Zeman, M.; Dam, B.; Van De Krol, R. Efficient solar water splitting by enhanced charge separation in a bismuth vanadate-silicon tandem photoelectrode. *Nat. Commun.* **2013**, *4*, 2195. [[CrossRef](#)] [[PubMed](#)]
7. Dong, W.; Guo, Y.; Guo, B.; Li, H.; Liu, H.; Joel, T.W. Enhanced photovoltaic effect in BiVO<sub>4</sub> semiconductor by incorporation with an ultrathin BiFeO<sub>3</sub> ferroelectric layer. *ACS Appl. Mater. Interfaces* **2013**, *5*, 6925–6929. [[CrossRef](#)] [[PubMed](#)]
8. Kim, T.W.; Choi, K.-S. Nanoporous BiVO<sub>4</sub> photoanodes with dual-layer oxygen evolution catalysts for solar water splitting. *Science* **2014**, *343*, 1245026. [[CrossRef](#)] [[PubMed](#)]
9. Zhang, L.; Herrmann, L.O.; Baumberg, J.J. Size dependent plasmonic effect on BiVO<sub>4</sub> photoanodes for solar water splitting. *Sci. Rep.* **2015**, *5*, 16660. [[CrossRef](#)] [[PubMed](#)]
10. Jeong, S.Y.; Choi, K.S.; Shin, H.-M.; Kim, T.L.; Song, J.; Yoon, S.; Jang, H.W.; Yoon, M.-H.; Jeon, C.; Lee, J. Enhanced photocatalytic performance depending on morphology of bismuth vanadate thin film synthesized by pulsed laser deposition. *ACS Appl. Mater. Interfaces* **2016**, *9*, 505–512. [[CrossRef](#)] [[PubMed](#)]
11. Grigioni, I.; Stampelcoskie, K.G.; Jara, D.H.; Dozzi, M.V.; Oriana, A.; Cerullo, G.; Kamat, P.V.; Selli, E. Wavelength-dependent ultrafast charge carrier separation in the WO<sub>3</sub>/BiVO<sub>4</sub> coupled system. *ACS Energy Lett.* **2017**, *2*, 1362–1367. [[CrossRef](#)]
12. Song, H.; Li, C.; Van, C.N.; Dong, W.; Qi, R.; Zhang, Y.; Huang, R.; Chu, Y.-H.; Duan, C.-G. Role of indium tin oxide electrode on the microstructure of self-assembled WO<sub>3</sub>-BiVO<sub>4</sub> hetero nanostructures. *J. Appl. Phys.* **2017**, *122*, 175301. [[CrossRef](#)]
13. Song, J.; Cha, J.; Lee, M.G.; Jeong, H.W.; Seo, S.; Yoo, J.A.; Kim, T.L.; Lee, J.; No, H.; Jeong, S.Y. Template-engineered epitaxial BiVO<sub>4</sub> photoanodes for efficient solar water splitting. *J. Mater. Chem. A* **2017**, *5*, 18831–18838. [[CrossRef](#)]
14. Wang, S.; Chen, P.; Yun, J.H.; Hu, Y.; Wang, L. An electrochemically treated BiVO<sub>4</sub> photoanode for efficient photoelectrochemical water splitting. *Angew. Chem. Int. Ed.* **2017**, *56*, 8500–8504. [[CrossRef](#)] [[PubMed](#)]
15. Han, H.S.; Shin, S.; Kim, D.H.; Park, I.J.; Kim, J.S.; Huang, P.-S.; Lee, J.-K.; Cho, I.S.; Zheng, X. Boosting the solar water oxidation performance of a BiVO<sub>4</sub> photoanode by crystallographic orientation control. *Energy Environ. Sci.* **2018**, *11*, 1299–1306. [[CrossRef](#)]
16. Jeong, S.Y.; Shin, H.-M.; Jo, Y.-R.; Kim, Y.J.; Kim, S.; Lee, W.-J.; Lee, G.J.; Song, J.; Moon, B.J.; Seo, S. Plasmonic silver nanoparticle-impregnated nanocomposite BiVO<sub>4</sub> photoanode for plasmon-enhanced photocatalytic water splitting. *J. Phys. Chem. C* **2018**, *122*, 7088–7093. [[CrossRef](#)]
17. Kim, S.; Yu, Y.; Jeong, S.Y.; Lee, M.G.; Jeong, H.W.; Kwon, Y.M.; Baik, J.M.; Park, H.; Jang, H.W.; Lee, S. Plasmonic gold nanoparticles-decorated BiVO<sub>4</sub>/ZnO nanowire heterostructure photoanodes for efficient water oxidation. *Catal. Sci. Technol.* **2018**. [[CrossRef](#)]
18. Li, J.; Guo, L.; Zhou, J.; Song, Q.; Liang, Z. Enhancing the photoelectrochemical performance of BiVO<sub>4</sub> by decorating only its (040) facet with self-assembled Ag@AgCl QDs. *J. Solid State Electron.* **2018**, 1–10. [[CrossRef](#)]
19. Song, J.; Seo, M.J.; Lee, T.H.; Jo, Y.-R.; Lee, J.; Kim, T.L.; Kim, S.-Y.; Kim, S.-M.; Jeong, S.Y.; An, H. Tailoring crystallographic orientations to substantially enhance charge separation efficiency in anisotropic BiVO<sub>4</sub> photoanodes. *ACS Catal.* **2018**, *8*, 5952–5962. [[CrossRef](#)]
20. Zhou, C.; Wang, S.; Zhao, Z.; Shi, Z.; Yan, S.; Zou, Z. A facet-dependent schottky-junction electron shuttle in a BiVO<sub>4</sub> {010}-Au-Cu<sub>2</sub>O Z-scheme photocatalyst for efficient charge separation. *Adv. Funct. Mater.* **2018**, *28*, 1801214. [[CrossRef](#)]

21. Park, Y.; McDonald, K.J.; Choi, K.-S. Progress in bismuth vanadate photoanodes for use in solar water oxidation. *Chem. Soc. Rev.* **2013**, *42*, 2321–2337. [[CrossRef](#)] [[PubMed](#)]
22. Kim, T.L.; Choi, M.-J.; Jang, H.W. Boosting interfacial charge transfer for efficient water-splitting photoelectrodes: Progress in bismuth vanadate photoanodes using various strategies. *MRS Commun.* **2018**, 1–14. [[CrossRef](#)]
23. Lee, M.G.; Moon, C.W.; Park, H.; Sohn, W.; Kang, S.B.; Lee, S.; Choi, K.J.; Jang, H.W. Dominance of plasmonic resonant energy transfer over direct electron transfer in substantially enhanced water oxidation activity of BiVO<sub>4</sub> by shape-controlled Au nanoparticles. *Small* **2017**, *13*, 1701644. [[CrossRef](#)] [[PubMed](#)]
24. Abdi, F.F.; Starr, D.E.; Ahmet, I.Y.; van de Krol, R. Photocurrent enhancement by spontaneous formation of a p-n junction in Ca-doped bismuth vanadate photoelectrodes. *ChemPlusChem* **2018**. [[CrossRef](#)]
25. Pendlebury, S.R.; Barroso, M.; Cowan, A.J.; Sivula, K.; Tang, J.; Grätzel, M.; Klug, D.; Durrant, J.R. Dynamics of photogenerated holes in nanocrystalline  $\alpha$ -Fe<sub>2</sub>O<sub>3</sub> electrodes for water oxidation probed by transient absorption spectroscopy. *Chem. Commun.* **2011**, *47*, 716–718. [[CrossRef](#)] [[PubMed](#)]
26. Zhong, D.K.; Cornuz, M.; Sivula, K.; Grätzel, M.; Gamelin, D.R. Photo-assisted electrodeposition of cobalt-phosphate (Co-Pi) catalyst on hematite photoanodes for solar water oxidation. *Energy Environ. Sci.* **2011**, *4*, 1759–1764. [[CrossRef](#)]
27. Klahr, B.; Gimenez, S.; Fabregat-Santiago, F.; Bisquert, J.; Hamann, T.W. Photoelectrochemical and impedance spectroscopic investigation of water oxidation with “Co-Pi”-coated hematite electrodes. *J. Am. Chem. Soc.* **2012**, *134*, 16693–16700. [[CrossRef](#)] [[PubMed](#)]
28. Grave, D.A.; Klotz, D.; Kay, A.; Dotan, H.; Gupta, B.; Visoly-Fisher, I.; Rothschild, A. Effect of orientation on bulk and surface properties of Sn-doped hematite ( $\alpha$ -Fe<sub>2</sub>O<sub>3</sub>) heteroepitaxial thin film photoanodes. *J. Phys. Chem. C* **2016**, *120*, 28961–28970. [[CrossRef](#)]
29. Hajibabaei, H.; Gao, Y.; Hamann, T.W. *Advances in Photoelectrochemical Water Splitting: Theory, Experiment and Systems Analysis (Energy and Environment Series)*, 1st ed.; Royal Society of Chemistry: Cambridge, UK, 2018; pp. 100–127, ISBN 1782629254.
30. Li, W.; Yang, K.R.; Yao, X.; He, Y.; Dong, Q.; Brudvig, G.W.; Batista, V.S.; Wang, D. Facet-dependent kinetics and energetics of hematite for solar water oxidation reactions. *ACS Appl. Mater. Interfaces* **2018**. [[CrossRef](#)] [[PubMed](#)]
31. Grave, D.A.; Yatom, N.; Ellis, D.S.; Toroker, M.C.; Rothschild, A. The “rust” challenge: On the correlations between electronic structure, excited state dynamics, and photoelectrochemical performance of hematite photoanodes for solar water splitting. *Adv. Mater.* **2018**, 1706577. [[CrossRef](#)] [[PubMed](#)]
32. Archana, P.S.; Pachauri, N.; Shan, Z.; Pan, S.; Gupta, A. Plasmonic enhancement of photoactivity by gold nanoparticles embedded in hematite films. *J. Phys. Chem. C* **2015**, *119*, 15506–15516. [[CrossRef](#)]
33. Quynh, L.T.; Van, C.N.; Bitla, Y.; Chen, J.W.; Do, T.H.; Tzeng, W.Y.; Liao, S.C.; Tsai, K.A.; Chen, Y.C.; Wu, C.L. Self-assembled BiFeO<sub>3</sub>- $\epsilon$ -Fe<sub>2</sub>O<sub>3</sub> vertical heteroepitaxy for visible light photoelectrochemistry. *Adv. Energy Mater.* **2016**, *6*, 1600686. [[CrossRef](#)]
34. Xie, J.; Guo, C.; Yang, P.; Wang, X.; Liu, D.; Li, C.M. Bi-functional ferroelectric BiFeO<sub>3</sub> passivated BiVO<sub>4</sub> photoanode for efficient and stable solar water oxidation. *Nano Energy* **2017**, *31*, 28–36. [[CrossRef](#)]
35. Song, J.; Kim, T.L.; Lee, J.; Cho, S.Y.; Cha, J.; Jeong, S.Y.; An, H.; Kim, W.S.; Jung, Y.-S.; Park, J. Domain-engineered BiFeO<sub>3</sub> thin-film photoanodes for highly enhanced ferroelectric solar water splitting. *Nano Res.* **2018**, *11*, 642–655. [[CrossRef](#)]
36. Linic, S.; Christopher, P.; Ingram, D.B. Plasmonic-metal nanostructures for efficient conversion of solar to chemical energy. *Nat. Mater.* **2011**, *10*, 911–921. [[CrossRef](#)] [[PubMed](#)]
37. Zhang, X.; Chen, Y.L.; Liu, R.-S.; Tsai, D.P. Plasmonic photocatalysis. *Rep. Prog. Phys.* **2013**, *76*, 046401. [[CrossRef](#)] [[PubMed](#)]
38. Kleemann, W. Absorption of colloidal silver in KCl. *Z. Phys.* **1968**, *215*, 113–120. [[CrossRef](#)]
39. Russell, B.K.; Mantovani, J.; Anderson, V.; Warmack, R.; Ferrell, T. Experimental test of the mie theory for microlithographically produced silver spheres. *Phys. Rev. B* **1987**, *35*, 2151. [[CrossRef](#)]
40. Mock, J.J.; Smith, D.R.; Schultz, S. Local refractive index dependence of plasmon resonance spectra from individual nanoparticles. *Nano Lett.* **2003**, *3*, 485–491. [[CrossRef](#)]
41. Park, J.; Kim, H.J.; Nam, S.; Kim, H.; Choi, H.-J.; Jang, Y.J.; Lee, J.S.; Shin, J.; Lee, H.; Baik, J.M. Two-dimensional metal-dielectric hybrid-structured film with titanium oxide for enhanced visible light absorption and photo-catalytic application. *Nano Energy* **2016**, *21*, 115–122. [[CrossRef](#)]

42. Li, H.; Li, Z.; Yu, Y.; Ma, Y.; Yang, W.; Wang, F.; Yin, X.; Wang, X. Surface-plasmon-resonance-enhanced photoelectrochemical water splitting from au-nanoparticle-decorated 3D TiO<sub>2</sub> nanorod architectures. *J. Phys. Chem. C* **2017**, *121*, 12071–12079. [[CrossRef](#)]
43. Awazu, K.; Fujimaki, M.; Rockstuhl, C.; Tominaga, J.; Murakami, H.; Ohki, Y.; Yoshida, N.; Watanabe, T. A plasmonic photocatalyst consisting of silver nanoparticles embedded in titanium dioxide. *J. Am. Chem. Soc.* **2008**, *130*, 1676–1680. [[CrossRef](#)] [[PubMed](#)]
44. Huang, L.; Chen, P.-C.; Liu, M.; Fu, X.; Gordiichuk, P.; Yu, Y.; Wolverson, C.; Kang, Y.; Mirkin, C.A. Catalyst design by scanning probe block copolymer lithography. *Proc. Natl. Acad. Sci. USA* **2018**, *115*, 3764–3769. [[CrossRef](#)] [[PubMed](#)]
45. Low, J.; Yu, J.; Jaroniec, M.; Wageh, S.; Al-Ghamdi, A.A. Heterojunction photocatalysts. *Adv. Mater.* **2017**, *29*, 1601694. [[CrossRef](#)] [[PubMed](#)]
46. Hurst, J.K. In pursuit of water oxidation catalysts for solar fuel production. *Science* **2010**, *328*, 315–316. [[CrossRef](#)] [[PubMed](#)]
47. Chen, S.; Wang, L.-W. Thermodynamic oxidation and reduction potentials of photocatalytic semiconductors in aqueous solution. *Chem. Mater.* **2012**, *24*, 3659–3666. [[CrossRef](#)]
48. Abdi, F.F.; van de Krol, R. Nature and light dependence of bulk recombination in Co-Pi-catalyzed BiVO<sub>4</sub> photoanodes. *J. Phys. Chem. C* **2012**, *116*, 9398–9404. [[CrossRef](#)]
49. Tang, F.; Cheng, W.; Su, H.; Zhao, X.; Liu, Q. Smoothing surface trapping states in 3D coral-like cooh-wrapped-BiVO<sub>4</sub> for efficient photoelectrochemical water oxidation. *ACS Appl. Mater. Interfaces* **2018**, *10*, 6228–6234. [[CrossRef](#)] [[PubMed](#)]
50. Chrisey, D.B.; Hubler, G.K. *Pulsed Laser Deposition of Thin Films*, 1st ed.; Wiley: New York, NY, USA, 1994; ISBN 0471592188.
51. Ashfold, M.N.; Claeysens, F.; Fuge, G.M.; Henley, S.J. Pulsed laser ablation and deposition of thin films. *Chem. Soc. Rev.* **2004**, *33*, 23–31. [[CrossRef](#)] [[PubMed](#)]
52. MacManus-Driscoll, J.L. Self-assembled heteroepitaxial oxide nanocomposite thin film structures: Designing interface-induced functionality in electronic materials. *Adv. Funct. Mater.* **2010**, *20*, 2035–2045. [[CrossRef](#)]
53. Zhao, Z.; Li, Z.; Zou, Z. Electronic structure and optical properties of monoclinic clinobisvanite BiVO<sub>4</sub>. *Phys. Chem. Chem. Phys.* **2011**, *13*, 4746–4753. [[CrossRef](#)] [[PubMed](#)]
54. Liu, T.; Zhou, X.; Dupuis, M.; Li, C. The nature of photogenerated charge separation among different crystal facets of BiVO<sub>4</sub> studied by density functional theory. *Phys. Chem. Chem. Phys.* **2015**, *17*, 23503–23510. [[CrossRef](#)] [[PubMed](#)]
55. Shirai, K.; Fazio, G.; Sugimoto, T.; Selli, D.; Ferraro, L.; Watanabe, K.; Haruta, M.; Ohtani, B.; Kurata, H.; Di Valentin, C. Water-assisted hole trapping at the highly curved surface of nano-TiO<sub>2</sub> photocatalyst. *J. Am. Chem. Soc.* **2018**, *140*, 1415–1422. [[CrossRef](#)] [[PubMed](#)]
56. Stoughton, S.; Showak, M.; Mao, Q.; Koirala, P.; Hillsberry, D.; Sallis, S.; Kourkoutis, L.; Nguyen, K.; Piper, L.; Tenne, D. Adsorption-controlled growth of BiVO<sub>4</sub> by molecular-beam epitaxy. *APL Mater.* **2013**, *1*, 042112. [[CrossRef](#)]
57. Rettie, A.J.; Mozaffari, S.; McDaniel, M.D.; Pearson, K.N.; Ekerdt, J.G.; Markert, J.T.; Mullins, C.B. Pulsed laser deposition of epitaxial and polycrystalline bismuth vanadate thin films. *J. Phys. Chem. C* **2014**, *118*, 26543–26550. [[CrossRef](#)]
58. Chien, N.V.; Chang, W.S.; Chen, J.-W.; Tsai, K.-A.; Tzeng, W.-Y.; Lin, Y.-C.; Kuo, H.-H.; Liu, H.-J.; Chang, K.-D.; Chou, W.-C. Heteroepitaxial approach to explore charge dynamics across Au/BiVO<sub>4</sub> interface for photoactivity enhancement. *Nano Energy* **2015**, *15*, 625–633. [[CrossRef](#)]
59. Chien, N.V.; Do, T.H.; Chen, J.-W.; Tzeng, W.-Y.; Tsai, K.-A.; Song, H.; Liu, H.-J.; Lin, Y.-C.; Chen, Y.-C.; Wu, C.-L. WO<sub>3</sub> mesocrystal-assisted photoelectrochemical activity of BiVO<sub>4</sub>. *NPG Asia Mater.* **2017**, *9*, e357. [[CrossRef](#)]
60. Zhang, W.; Yan, D.; Tong, X.; Liu, M. Ultrathin lutetium oxide film as an epitaxial hole-blocking layer for crystalline bismuth vanadate water splitting photoanodes. *Adv. Funct. Mater.* **2018**, *28*, 1705512. [[CrossRef](#)]
61. Zhang, W.; Yan, D.; Li, J.; Wu, Q.; Cen, J.; Zhang, L.; Orlov, A.; Xin, H.; Tao, J.; Liu, M. Anomalous conductivity tailored by domain-boundary transport in crystalline bismuth vanadate photoanodes. *Chem. Mater.* **2018**, *30*, 1677–1685. [[CrossRef](#)]

62. Rettie, A.J.; Lee, H.C.; Marshall, L.G.; Lin, J.-F.; Capan, C.; Lindemuth, J.; McCloy, J.S.; Zhou, J.; Bard, A.J.; Mullins, C.B. Combined charge carrier transport and photoelectrochemical characterization of BiVO<sub>4</sub> single crystals: Intrinsic behavior of a complex metal oxide. *J. Am. Chem. Soc.* **2013**, *135*, 11389–11396. [[CrossRef](#)] [[PubMed](#)]
63. Rettie, A.J.; Chemelewski, W.D.; Lindemuth, J.; McCloy, J.S.; Marshall, L.G.; Zhou, J.; Emin, D.; Mullins, C.B. Anisotropic small-polaron hopping in W:BiVO<sub>4</sub> single crystals. *Appl. Phys. Lett.* **2015**, *106*, 022106. [[CrossRef](#)]
64. Pintlilie, L.; Alexe, M. Metal-ferroelectric-metal heterostructures with schottky contacts. I. Influence of the ferroelectric properties. *J. Appl. Phys.* **2005**, *98*, 124103. [[CrossRef](#)]
65. Pantel, D.; Chu, Y.-H.; Martin, L.W.; Ramesh, R.; Hesse, D.; Alexe, M. Switching kinetics in epitaxial BiFeO<sub>3</sub> thin films. *J. Appl. Phys.* **2010**, *107*, 084111. [[CrossRef](#)]
66. Hauser, A.; Zhang, J.; Mier, L.; Ricciardo, R.; Woodward, P.; Gustafson, T.; Brillson, L.; Yang, F. Characterization of electronic structure and defect states of thin epitaxial BiFeO<sub>3</sub> films by UV-visible absorption and cathodoluminescence spectroscopies. *Appl. Phys. Lett.* **2008**, *92*, 222901. [[CrossRef](#)]
67. Yi, H.; Choi, T.; Choi, S.; Oh, Y.S.; Cheong, S.W. Mechanism of the switchable photovoltaic effect in ferroelectric BiFeO<sub>3</sub>. *Adv. Mater.* **2011**, *23*, 3403–3407. [[CrossRef](#)] [[PubMed](#)]
68. Liu, Q.; Zhou, Y.; You, L.; Wang, J.; Shen, M.; Fang, L. Enhanced ferroelectric photoelectrochemical properties of polycrystalline BiFeO<sub>3</sub> film by decorating with ag nanoparticles. *Appl. Phys. Lett.* **2016**, *108*, 022902. [[CrossRef](#)]
69. Ji, W.; Yao, K.; Lim, Y.-F.; Liang, Y.C.; Suwardi, A. Epitaxial ferroelectric BiFeO<sub>3</sub> thin films for unassisted photocatalytic water splitting. *Appl. Phys. Lett.* **2013**, *103*, 062901. [[CrossRef](#)]
70. Rong, N.; Chu, M.; Tang, Y.; Zhang, C.; Cui, X.; He, H.; Zhang, Y.; Xiao, P. Improved photoelectrocatalytic properties of Ti-doped BiFeO<sub>3</sub> films for water oxidation. *J. Mater. Sci.* **2016**, *51*, 5712–5723. [[CrossRef](#)]
71. Moniz, S.J.; Quesada-Cabrera, R.; Blackman, C.S.; Tang, J.; Southern, P.; Weaver, P.M.; Carmalt, C.J. A simple, low-cost CVD route to thin films of BiFeO<sub>3</sub> for efficient water photo-oxidation. *J. Mater. Chem. A* **2014**, *2*, 2922–2927. [[CrossRef](#)]
72. Cao, D.; Wang, Z.; Wen, L.; Mi, Y.; Lei, Y. Switchable charge-transfer in the photoelectrochemical energy-conversion process of ferroelectric BiFeO<sub>3</sub> photoelectrodes. *Angew. Chem. Int. Ed.* **2014**, *53*, 11027–11031. [[CrossRef](#)] [[PubMed](#)]
73. Huang, Y.-L.; Chang, W.S.; Chien, N.V.; Liu, H.-J.; Tsai, K.-A.; Chen, J.-W.; Kuo, H.-H.; Tzeng, W.-Y.; Chen, Y.-C.; Wu, C.-L. Tunable photoelectrochemical performance of Au/BiFeO<sub>3</sub> heterostructure. *Nanoscale* **2016**, *8*, 15795–15801. [[CrossRef](#)] [[PubMed](#)]
74. Wu, J.; Wang, J. Orientation dependence of ferroelectric behavior of BiFeO<sub>3</sub> thin films. *J. Appl. Phys.* **2009**, *106*, 104111. [[CrossRef](#)]
75. Li, J.; Wang, J.; Wuttig, M.; Ramesh, R.; Wang, N.; Ruetter, B.; Pyatakov, A.P.; Zvezdin, A.; Viehland, D. Dramatically enhanced polarization in (001), (101), and (111) BiFeO<sub>3</sub> thin films due to epitaxial-induced transitions. *Appl. Phys. Lett.* **2004**, *84*, 5261–5263. [[CrossRef](#)]
76. Sone, K.; Naganuma, H.; Miyazaki, T.; Nakajima, T.; Okamura, S. Crystal structures and electrical properties of epitaxial BiFeO<sub>3</sub> thin films with (001), (110), and (111) orientations. *Jpn. J. Appl. Phys.* **2010**, *49*, 09MB03. [[CrossRef](#)]
77. Baek, S.H.; Folkman, C.M.; Park, J.W.; Lee, S.; Bark, C.W.; Tybell, T.; Eom, C.B. The nature of polarization fatigue in BiFeO<sub>3</sub>. *Adv. Mater.* **2011**, *23*, 1621–1625. [[CrossRef](#)] [[PubMed](#)]
78. Das, R.; Kim, D.; Baek, S.; Eom, C.; Zavaliche, F.; Yang, S.; Ramesh, R.; Chen, Y.; Pan, X.; Ke, X. Synthesis and ferroelectric properties of epitaxial BiFeO<sub>3</sub> thin films grown by sputtering. *Appl. Phys. Lett.* **2006**, *88*, 242904. [[CrossRef](#)]
79. Yang, W.; Yu, Y.; Starr, M.B.; Yin, X.; Li, Z.; Kvit, A.; Wang, S.; Zhao, P.; Wang, X. Ferroelectric polarization-enhanced photoelectrochemical water splitting in TiO<sub>2</sub>-BaTiO<sub>3</sub> core-shell nanowire photoanodes. *Nano Lett.* **2015**, *15*, 7574–7580. [[CrossRef](#)] [[PubMed](#)]

